Synoptic-scale transport of reactive nitrogen over the western Pacific in spring

Y. Miyazaki,[1] Y. Kondo,[1] M. Koike,[2] H. E. Fuelberg,[3] C. M. Kiley,[3] K. Kita,[4] N. Takegawa,[1] G. W. Sachse,[5] F. Flocke,[6] A. J. Weinheimer,[6] H. B. Singh,[7] F. L. Eisele,[6,9] M. Zondlo,[6] R. W. Talbot,[8] S. T. Sandholm,[9] M. A. Avery,[5] and D. R. Blake[10]

Received 29 November 2002; revised 20 March 2003; accepted 2 May 2003; published 3 September 2003.

[1] Pathways of synoptic-scale uplifted transport of pollutants from East Asia and their effects on chemical distributions of NO_y species are investigated based on a subset of the aircraft data obtained during the NASA Transport and Chemical Evolution over the Pacific (TRACE-P) experiment, conducted in February–April 2001. Meteorological and chemical analyses indicate that 73% of the uplifted transport was associated with warm conveyor belts (WCBs) and convective outflow (COF), which transported air masses strongly impacted by biomass burning over Southeast Asia. The rest (27%) of the uplifted air masses originated over coastal regions of northeast China, where fossil fuel combustion was a dominant source of pollutants. Both WCB associated with a midlatitude cyclone and COF associated with a stationary front over southeast China are examined in detail for the April 4 case. During the TRACE-P period, low $NO_x(= NO + NO_2)/NO_y$ ratios in the WCB and COF indicate that a significant part of the NO_x was oxidized to nitric acid (HNO_3) and peroxyacetyl nitrate (PAN) during transport. Low HNO_3/NO_y ratios in the WCB and COF airstreams indicate that a large amount of HNO_3 was removed during transport on timescales within 1–3 days. PAN was found to be the dominant form of NO_y in air masses transported by the WCB and COF, likely due to the production of PAN in regions of biomass burning and industrial emissions, as well as due to the rapid removal of HNO_3 during transport. For emissions that were transported to the free troposphere by WCBs and COF, about 10–20% of the NO_y remained after transport to the free troposphere, and 30% of the NO_y surviving in the boundary layer in limited cases. The results indicate that the WCB and COF provide both an efficient sink for HNO_3 and an efficient mechanism for the transport of PAN from the boundary layer to the free troposphere over the western Pacific. *INDEX TERMS:* 0368 Atmospheric Composition and Structure: Troposphere—constituent transport and chemistry; 0322 Atmospheric Composition and Structure: Constituent sources and sinks; 0345 Atmospheric Composition and Structure: Pollution—urban and regional (0305); *KEYWORDS:* warm conveyor belts, convection, reactive nitrogen, TRACE-P, western Pacific

Citation: Miyazaki, Y., et al., Synoptic-scale transport of reactive nitrogen over the western Pacific in spring, *J. Geophys. Res.*, *108*(D20), 8788, doi:10.1029/2002JD003248, 2003.

1. Introduction

[2] Midlatitude cyclones have been recognized to play a key role in redistributing trace species and affecting their chemical evolution in the troposphere. Airstreams associated with midlatitude cyclones, such as Warm Conveyor Belts (WCBs) and Dry Airstreams (DAs), are of great importance. The WCB is an ascending airstream ahead of a surface cold front, traveling into the middle to upper troposphere [e.g., *Browning and Roberts*, 1994], which transports trace species from the boundary layer to the free troposphere.

[3] Recently, characteristics of these airstream types associated with midlatitude cyclones have been studied, especially from a viewpoint of the effects of transport on trace species. *Bethan et al.* [1998] interpreted chemical and meteorological data in the context of the airstreams within cyclones over the eastern North Atlantic Ocean (NAO) in spring. They concluded that the conveyor belts within

[1]Research Center for Advanced Science and Technology, University of Tokyo, Tokyo, Japan.
[2]Earth and Planetary Science, Graduate School of Science, University of Tokyo, Tokyo, Japan.
[3]Department of Meteorology, Florida State University, Tallahassee, Florida, USA.
[4]Department of Environmental Science, Ibaraki University, Ibaraki, Japan.
[5]NASA Langley Research Center, Hampton, Virginia, USA.
[6]National Center for Atmospheric Research, Boulder, Colorado, USA.
[7]NASA Ames Research Center, Moffett Field, California, USA.
[8]University of New Hampshire, Durham, New Hampshire, USA.
[9]Georgia Institute of Technology, Atlanta, Georgia, USA.
[10]University of California, Irvine, Irvine, California, USA.

0148-0227/03/2002JD003248$09.00

cyclones are capable of effectively transporting boundary layer air to the free troposphere. *Kowol-Santen et al.* [2001] showed that up to ~70% of carbon monoxide (CO) in the boundary layer can be transported to the free troposphere in the region of WCBs, using a mesoscale model. The chemical characteristics of CO, ozone (O_3), and total reactive nitrogen (NO_y) were studied more systematically for these airstreams associated with midlatitude cyclones over the NAO, based on aircraft measurements [*Cooper et al.*, 2002a, 2002b].

[4] The chemical compositions in the airstreams are controlled mainly by two factors: the geographic distribution of sources and the cyclone pathway. For example, air masses in WCBs vary from fairly clean [*Grant et al.*, 2000] to highly polluted [*Stohl and Trickl*, 1999], depending on their origins. East Asia also experiences midlatitude cyclones [e.g., *Chen et al.*, 1991, 1992]. In fact, *Stohl* [2001] has shown that WCB air masses originate most frequently in the boundary layer over the warm water pools in East Asia, similarly to northeast America, based on a large number of trajectory calculations.

[5] The export of NO_y from the boundary layer to the free troposphere is a key parameter of the global O_3 budget. *Liang et al.* [1998] showed that the influence of NO_y exported from the U.S. boundary layer on the global O_3 budget is greater than the influence of direct O_3 transport, by using a three-dimensional (3-D) chemical transport model (CTM). Considering the large emissions of reactive nitrogen over the Asian continent [*Streets et al.*, 2003], transport of NO_y from the continental boundary layer over Asia to the western Pacific should be of great importance. In 3-D CTM studies, *Bey et al.* [2001] found that frontal lifting plays a critical role in controlling the chemical characteristics of the Asian outflow in February–March. In fact, cumulus convection associated with a cold front over northeast China has been shown with aircraft measurements to transport highly polluted air to the upper troposphere over the Japan Sea in April [*Miyazaki et al.*, 2002]. There are still, however, large uncertainties in our knowledge concerning the emission rates, chemical processes, and transport processes of NO_y species [*Stohl et al.*, 2002].

[6] In this study, the chemical data obtained during the NASA Transport and Chemical Evolution over the Pacific (TRACE-P) experiment, conducted in February–April 2001, are used to investigate the chemical evolution of NO_y associated with upward transport due to convection and midlatitude cyclones over the western Pacific in spring. A major objective of this study is to examine pathways of uplifted airstreams from the Asian continent and to investigate the role of upward transport in controlling the distributions of NO_y species. For this purpose, we focus on uplifted patterns of transport from the boundary layer over the continent. In addition, the chemical evolution of NO_y species is examined in detail within airstreams in the developing cyclones and convective outflow, based on aircraft measurements.

2. Data Description

[7] During TRACE-P, a variety of chemical species and meteorological parameters were measured on board the NASA P-3B and DC-8 aircraft. The instrumentation of the TRACE-P mission is described in an accompanying overview paper [*Jacob et al.*, 2003]. Measurement data and the instrumentation used in this study are summarized in Table 1. In this study, CO was used as a long-lived tracer in combination with trajectories for identifying airstreams. One-minute merged data were used for the P-3B, and the measured NO_y was used as total reactive nitrogen. For the DC-8 measurements, NO_y is defined as the sum of NO + NO_2 + PAN + HNO_3. Uncertainty associated with using the sum of these species as a surrogate for the total NO_y was estimated to be 14% from the median values and accuracy of each measurement. Alkyl nitrates and peroxypropionyl nitrate (PPN) constituted only 2–3% when they are included in the sum of the NO_y species for the DC-8 data. Since HNO_3 was measured on the DC-8 with a temporal resolution of 2 min, HNO_3 merged data were used for the DC-8 NO_y analysis. Table 2 summarizes the relationship between the measured NO_y and the sum of NO + NO_2 + PAN + HNO_3 for the P-3B. The data used here were obtained over 122°–170°E, 22°–42°N, which is the study area described in section 3.2. On average, 86% of NO_y at 2–6 km is accounted for as NO_x, PAN, and HNO_3. Although NO_y was not measured at 7–12 km during TRACE-P, *Kondo et al.* [1997a] and *Singh et al.* [1998] reported general agreement of the measured and the sum of NO_y with a small deficit (10–15%) at 6–12 km over the western Pacific based on data from PEM-West B, conducted in February–March 1994. The deficit of NO_y in this study can be explained mainly by alkyl nitrates [*Simpson et al.*, 2003; *Talbot et al.*, 2003] and aerosol nitrate (NO_3^-) [*Koike et al.*, 2003]. We do not include these data in this analysis because the time resolution of these species (typically 5–15 min) would make it difficult to discuss the NO_y in a selected air mass.

[8] In order to select vertically uplifted patterns of lagrangian transport from the Asian continent, 5-day back trajectories were used. The trajectories were calculated along the flight tracks of the P-3B and DC-8 at 5-min intervals by the Florida State University (FSU) Kinematic Trajectory Model [*Fuelberg et al.*, 1996]. The calculation used the European Centre for Medium-Range Weather Forecasts (ECMWF) data [*Fuelberg et al.*, 2003]. The data set has a 1° × 1° horizontal resolution and 61 sigma levels in the vertical, supplied at 6-hourly intervals throughout the TRACE-P period. Some limitations of the trajectory calculations are described in previous works [e.g., *Stohl et al.*, 1995]. Geostationary Meteorological Satellite-5 (GMS-5) infrared (IR) images were used for the identification of airstreams associated with cyclones. Images of average rainfall rates, using the Ferriday algorithm [*Ferriday and Avery*, 1994] on Special Sensor Microwave/Imager (SSM/I) satellite data, are available at the NOAA website http://www.etl.noaa.gov/satres/archive.html.

3. Transport Pathways From the Asian Continent During TRACE-P

3.1. Meteorological Conditions in February–April

[9] Brief highlights of the meteorological conditions in February–April during TRACE-P are described here, which are key points for this study. Meteorological conditions concerning atmospheric transport during TRACE-P are

Table 1. Species Used in This Study Measured Aboard the P-3B and DC-8 Aircraft During TRACE-P

Species	Aircraft	Technique	Accuracy	1σ Precision	Reference
CO	P-3B, DC-8	Differential absorption technique using a tunable diode laser	±2%	±1%	*Sachse et al.* [1987]
NO, NO_2, NO_y	P-3B	Chemiluminescence	±8%(NO), ±20% (NO_2), ±18%(NO_y)	±6pptv at 50pptv(NO), ±4pptv at 70pptv (NO_2), ±16pptv at 500 pptv(NO_y)	*Kondo et al.* [1997b], *Koike et al.* [2000]
NO, NO_2	DC-8	Photofragmentation two-photon laser-induced fluorescence	±20–30%	±20–30%	*Sandholm et al.* [1990]
PAN	P-3B	GC/ECD	±10%	±5%	
PAN	DC-8	GC/ECD	±25%	±10%	*Singh et al.* [1996]
HNO_3	P-3B	CIMS	±15–25%	±15–25%	*Mauldin et al.* [1998]
HNO_3	DC-8	Mist chamber technique	±10–20%	±10–20%	*Talbot et al.* [1997]
NMHCs/halocarbons	P-3B, DC-8	Grab sample/GC	±2–20%	±1–3%	*Blake et al.* [2001]

summarized by *Fuelberg et al.* [2003] in more detail. Figure 1 displays the time-averaged sea level pressure and rainfall rates derived from the SSM/I instrument in February–April 2001. Stationary fronts prevail in the convergence zones over central and southern China in early spring, the season that corresponds to the transition period from the winter to summer monsoons in Asia [*Nieuwolt*, 1977]. Incursions of warmer air from the south become more frequent due to the building up of the Pacific high-pressure system, while movement of cold air southward decreases because the Siberian High weakens by March, as seen in the left panels of Figure 1. As a result, the warming causes frequent convection in Southeast Asia [*Nieuwolt*, 1977; *Bey et al.*, 2001], indicated in the right panels of Figure 1. Moreover, a widespread region of precipitation over the western Pacific, as seen in Figure 1, is associated with pathways of midlatitude cyclones, as indicated by *Fuelberg et al* [2003]. They derived an average frequency of 3–4 midlatitude cyclones per week over the western Pacific during TRACE-P.

3.2. Trajectory Analyses

[10] In order to examine the export pathways of pollutants, vertically uplifted patterns of lagrangian transport were selected by using 5-day back trajectories of sampled air masses. We selected air masses that originated in the boundary layer (pressure levels greater than 800 hPa; altitudes below 2 km) over the Asian continent and that were transported above the 800-hPa level prior to the aircraft measurements. An uplifted air mass is defined here as that ascending at least 1 km. It should be noted that the boundary layer altitude can extend higher or lower depending on a variety of local conditions. Therefore the boundary layer in the current analysis is approximated by this range of altitudes. Figure 2a shows a horizontal plot of the selected trajectories, and a summary of these trajectories is listed in Table 3. Variations of height are also given as functions of longitude (Figure 2b) and time (Figure 2c). During the observational period between 7 March and 4 April, the uplifted transport pattern consists of 146 trajectories (90 from 9 DC-8 flights and 56 from 6 P-3B flights). The air masses were uplifted from the boundary layer within 1–3 days (Table 3 and Figure 2c). The study area in this analysis is defined to be over 122°–170°E, 22°–42°N, where the intensive flights were made from Hong Kong and Yokota.

[11] Locations where the trajectories reached the 800-hPa level are plotted in Figure 3, which represent estimated origins of the air masses. The results show that 73% of the selected trajectories originated over a broad region in Southeast Asia (SA) where frequent convective activities occurred during the TRACE-P period, as revealed by abundant satellite-derived precipitation and lightning observations (see Figure 1 and also *Fuelberg et al.* [2003]). The SA region corresponds to the location where extensive biomass burning occurred during the observational season. This will be further examined in section 3.3. On the other hand, 27% of the selected trajectories showed the air masses originated in the northeast coastal region of China (NC) at 30°–40°N.

[12] Individual trajectories were also compared with cloud images observed by the GMS and with surface weather charts. In this study, WCB airstreams were distinguished from other uplifted transport, i.e., convection. For instance, *Stohl and Trickl* [1999] have defined WCBs as airstreams ascending at least 8 km in 60 hours, using coherent ensembles of trajectories (CETs) methods [*Wernli and Davis*, 1997] with PV fields and cloud images. In this analysis, airstreams associated with the WCB are defined as follows: first, cloud features associated with surface cold and warm fronts were examined in relation to the sampling location of the aircraft. Each back trajectory calculated along the flight track was then compared to the motion of the frontal system. If the trajectories run parallel to the surface cold front and ascend at least 1 km within 24 hours, the corresponding airstream was identified as a WCB. As a result, four individual WCBs within different cyclones were identified, consisting of 53 trajectories (36% of the uplifted trajectories). All of these WCBs originated in the SA region, with a mean ascent rate of 2.3 (±1.1) km/24 hours.

[13] Convective outflow (COF) was determined by trajectories that were uplifted over satellite-observed convective cloud regions and those identified with surface weather charts. The COF determined in this study includes convection such as that associated with a stationary front and that occurring behind a cold front. In addition, convection in advance of a cold front is also categorized as COF in this analysis. The results of this analysis show that 10 individual

Table 2. Mean and ± 1σ Standard Deviations of Ratios Between the Measured NO_y and the Sum of NO_x, PAN, and HNO_3 (Defined as $\Sigma(NO_y)_i$ on Board the P-3B

Altitude, km	$\Sigma(NO_y)_i/NO_y$	Number of Data Points
4–6	0.88 (± 0.14)	152
2–4	0.84 (± 0.19)	175
0–2	0.78 (± 0.22)	365

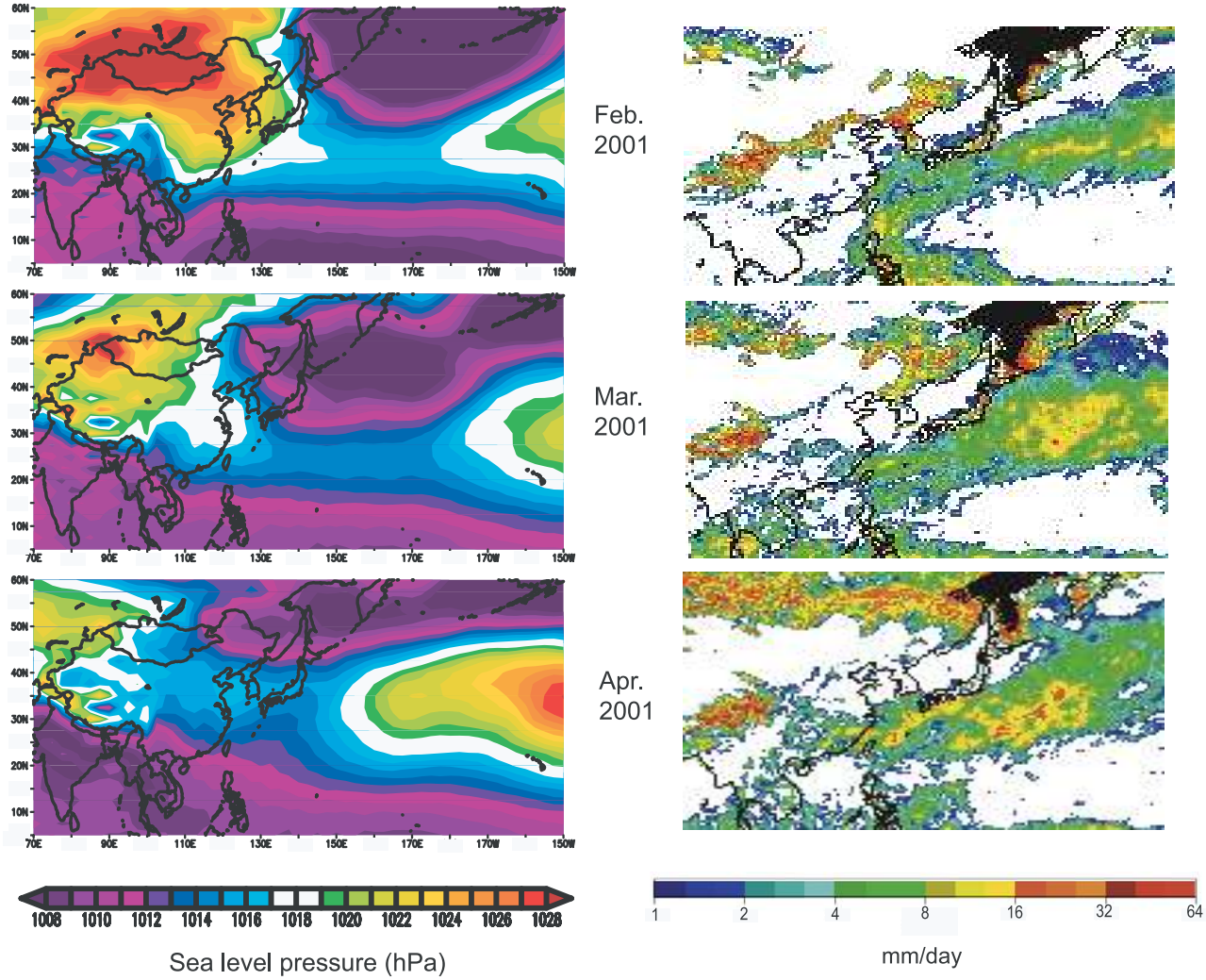

Figure 1. Mean sea level pressure (left) and satellite-derived rainfall rates from the SSM/I instrument (right) during February and April 2001.

COFs were identified, consisting of 80 trajectories (55% of the uplifted trajectories). Seven of the 10 COFs originated in the SA region, while the remaining three originated in the NC region. The mean ascent rate for COFs was 4.7 (±2.5) km/24 hours, which is faster than that of the WCBs by a factor of 2. It should be noted that the trajectories have limitations of spatial and temporal resolution relative to the much smaller scales of vertical transport, including convection. Some air masses may ascend much more rapidly in a convective cell than indicated by the relatively coarse resolution of the ECMWF data currently used. Thus the uplifted transport presented here might be a lower limit of upward transport in the real atmosphere. The remaining trajectories identified as neither WCB nor COF consist of only 9% of the total, most of which include outflows in the lower free troposphere. It should also be noted that the fractions of WCBs and COF to the total uplifted trajectories are not statistically representative due to a bias in the sampling locations and time.

3.3. Chemical Tracers of Source Description

[14] In addition to the frequent convection over Southeast Asia, distributions of pollutant emissions during the observational period are also important. Figure 4 shows the annual emission rates of CO and NO_x/CO molar ratios over Asia estimated for the year 2000 [*Streets et al.*, 2003]. These emission rates are given at http://www.cgrer.uiowa.edu/people/carmichael/ACESS/Emission-data_main.html. CO and NO_x are strongly emitted along the east and southeast coast of China (22°–44°N, 110°–122°E). Two major sources are considered in these estimates: biomass burning and industrial emissions. Extensive biomass burning occurs in Southeast Asia and northern India in the spring (February–April) [e.g., *Duncan et al.*, 2003], while industrial emissions are largest in northeast China [e.g., *Bey et al.*, 2001].

[15] In order to examine the signatures of the chemical tracers in the identified air masses, scatter plots among CO, CH_3Cl, and C_2Cl_4 are shown in Figure 5. In this analysis, CH_3Cl and C_2Cl_4 are used as tracers of biomass burning and fossil fuel combustion, respectively [e.g., *Wang et al.*, 1995; *Blake et al.*, 1996]. A tight, positive correlation between CO and CH_3Cl ($r^2 = 0.74$) is apparent in the airstreams in the SA category. A slope of the regression line (dCH_3Cl/dCO) of 0.52 (pptv/ppbv) is similar to the emission ratios of 0.50–0.57 (pptv/ppbv) [*Rudolph et al.*, 1995; *Andreae et al.*, 1996; *Blake et al.*, 1996] from biomass burning. In

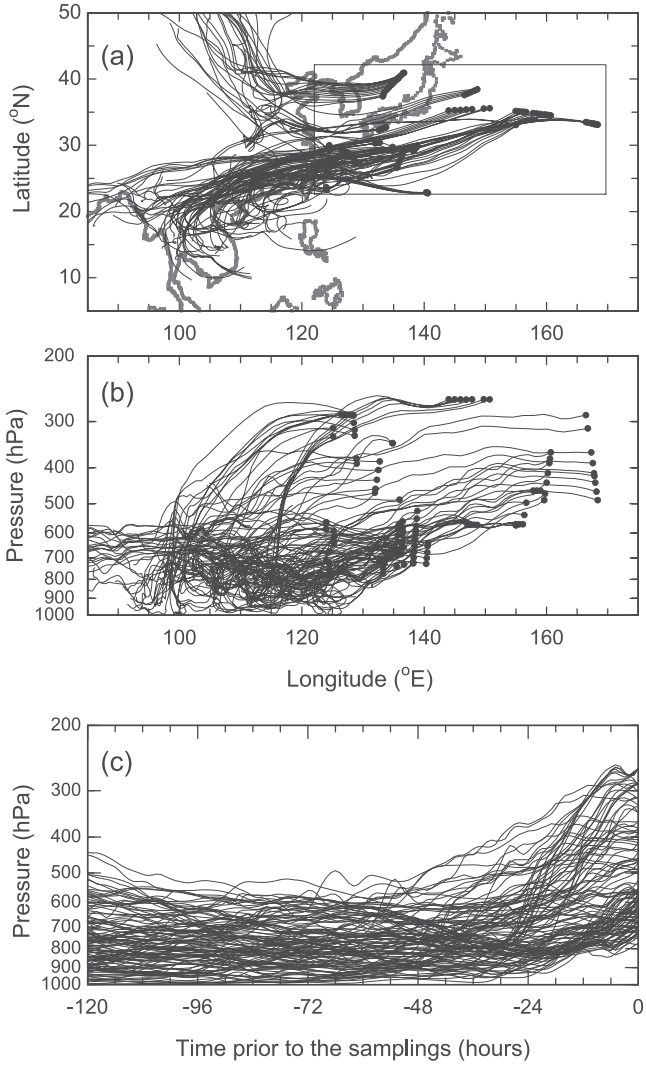

Figure 2. (a) Horizontal plot of 5-day back trajectories corresponding to uplifted airstreams from the boundary layer over the Asian continent. Dots indicate the aircraft sampling points along the flight tracks. A study area in this study is also shown. (b) Vertical changes of the trajectories corresponding to the uplifted airstreams as a function of longitude. (c) Same as Figure 2b but as a function of time prior to the samplings.

contrast, the correlation was much poorer in the NC category (r^2 = 0.34), with lower values of CH_3Cl (530–620 pptv) than those in the SA category (570–700 pptv). These results are consistent with the trajectory analysis, showing that the WCB and COF air masses originated from the intense biomass burning region.

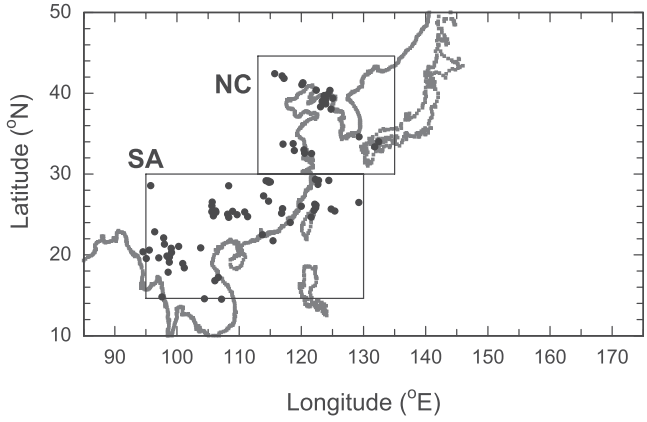

Figure 3. Horizontal plot of trajectory points in the uplifted category, locations of which were at the top of the boundary layer (~800 hPa).

[16] In contrast, the mixing ratios of C_2Cl_4 in the NC category (8–15 pptv) were higher than those in the SA category (3–10 pptv). The result indicates that the airstreams in the NC category were much more strongly influenced by fossil fuel combustion than those in the SA category. However, it is likely that the air masses influenced by fossil fuel combustion were mixed with the biomass burning plumes in the WCB and COF airstreams because CO was correlated with C_2Cl_4 (r^2 = 0.43).

4. WCB and COF on 4 April

4.1. Meteorological Conditions

[17] This section describes an example of two different pathways of upward transport: WCB and COF. Figure 6 shows GMS water vapor images with flight tracks for the P-3B and DC-8 and sea level pressure at 0000 UT on 4 April. There were two frontal systems over the western-to-central Pacific on this day. A developing wave cyclone (Cyclone-A) was centered near 50°N, 150°E, with a cold front extending southward. The other system was a deeply occluded low (Cyclone-B) located just west of Alaska. The upper level trough associated with Cyclone-A (not shown) corresponds to a dry region over Japan in the middle to upper troposphere. The P-3B flew from Yokota Air Force Base (AFB) (35°N, 140°E) to Midway Island (28°N, 177°E), conducting extensive in-progress vertical sampling at 0–6 km. The DC-8, which headed for Kona (19°N, 204°E), Hawaii, also followed the same route between Yokota and Midway at 0–11 km. Both aircraft crossed a cloud region associated with the surface cold front at 146°E. In order to obtain good vertical coverage of air samplings over the western Pacific, the P-3B made low-altitude

Table 3. Trajectory Data Used in This Study[a]

Altitude, hPa	Altitude, km	Median Latitude, °N	Median Longitude, °E	DC-8 + P-3B	Uplifted Trj	CO, ppbv	Average Times, days
350–200	8–12	35.3	146.0	358	20	200	2.3± 0.9
550–350	5–8	33.9	157.1	812	32	196	2.1± 0.8
800–550	2–5	30.1	135.7	1578	94	257	1.3± 0.9

[a]Values in the DC-8+P-3B column represent the total number of trajectories in the study area. Similarly, values in the uplifted Trj column represent the number of trajectories in the uplifted transport category. Average times are timescales from the top of the boundary layer to the sampling points derived from the trajectories.

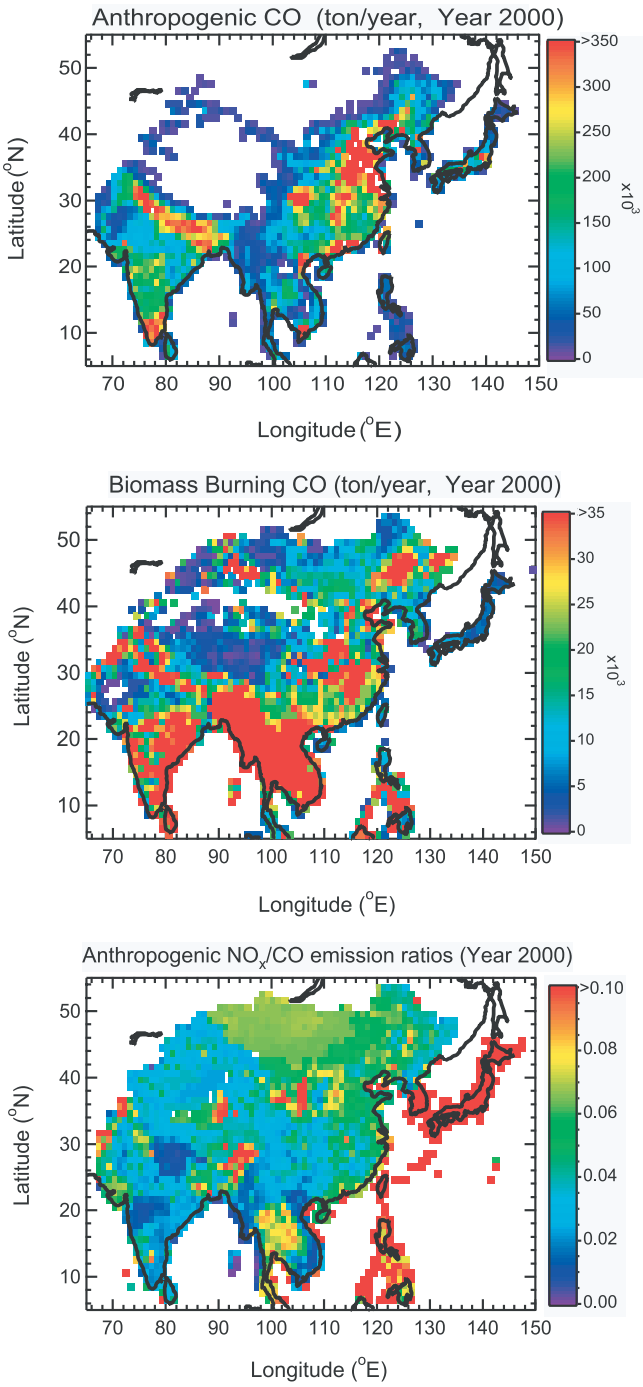

Figure 4. Emission estimates of CO and NO_x/CO molar ratios for year 2000 over East Asia compiled by *Streets et al.* [2003]. The data are available at the website http://www.cgrer.uiowa.edu/people/carmichael/ACESS/Emission-data_main.html.

measurements coinciding with the high-altitude measurements by the DC-8 and vice versa. Thus, the distributions of chemical species in a broad spatial range were obtained around the Cyclone-A.

4.2. Airstream Classification Associated With the Cyclone

[18] Figure 7 displays vertical and longitudinal distributions of measured CO along the flight tracks of the P-3B and DC-8. High CO values reaching 200 ppbv were observed at 5–10 km over a wide domain in the western Pacific at 142°–186°E. Air masses in each identified airstream are categorized as a (WCB), b (COF), and c (DA) at 5–10 km and are described in sections 4.2.1– 4.2.3.

4.2.1. Warm Conveyor Belt (WCB)

[19] Figure 8 shows the trajectories that represent a well-defined WCB airstream (Figure 7a). Air masses in the WCB were observed at 8°–20° east in longitude relative to the center of a cyclone, which were within a typical range of 0°–20° in the upper troposphere [*Cooper et al.*, 2002b]. As is typical for WCB trajectories [e.g., *Browning*, 1990], the trajectories move parallel to the surface cold front, ascending toward the northeast over the western Pacific. The mean timescale for transport from the top of the boundary layer to the sampling points was estimated to be 2.6±0.6 days, which was derived from trajectories. The mean ascent rate of the WCB was 2.3±0.9 km/24 hours, estimated from the trajectories. High relative humidity of 85 to nearly 100% (not shown) is consistent with upward transport. The median CO mixing ratios in the WCB air masses were 180–200 ppbv, reflecting the strong influence of high emissions of pollutants in the SA region. The CO values were higher than the median values of 140 ppbv in the WCB in the middle to upper troposphere over the western North Atlantic Ocean in spring [*Cooper et al.*, 2002b]. Trajectories in Figure 8 indicate that these air masses were strongly impacted by CO emissions over southeast China, including coastal regions, where the emissions of CO from biomass burning are large.

4.2.2. Convective Outflow (COF)

[20] Contrary to a typical WCB, the sampling points of the air masses shown in Figure 7b were located 0°–7° west in longitude relative to the center of Cyclone-A. These air masses were also polluted (CO mixing ratios > 200 ppbv) and humid (relative humidity of nearly 100%), indicating that they were also transported upward from the polluted boundary layer. The bulk of the trajectories shows mean ascending motion of the air masses in 1.3 ± 0.2 days from the boundary layer to the sampling points at 10 km, as seen in Figure 9. The ascent rate estimated from the trajectories was about 7.3 ± 1.7 km/24 hours, which was much faster than that of the WCB (2.3 ± 0.9 km/24 hours) described in section 4.2.1.

[21] Figure 10 shows the GMS water vapor image at 0200 UT on 3 April together with the location of a surface front 24 hours prior to sampling. A surface stationary front existed continuously at about 25°N over southeast China for approximately 3 days during 1 April and 4 April. Therefore the polluted air masses should have been rapidly lifted up to an altitude of 9–10 km by this stationary front and then transported cyclonically at this altitude along the eastern side of the upper-level trough located over the northern part of Japan.

[22] According to the trajectories, these air masses were found to originate in southeast China. As examined in section 3.3, correlation between CO and CH_3Cl (not shown) also confirms that the influence of biomass burning was dominant in these air masses. Because the air masses in the WCB were also identified as originating from the region of this stationary front, as discussed in the previous section, some air masses were lifted up by the stationary frontal

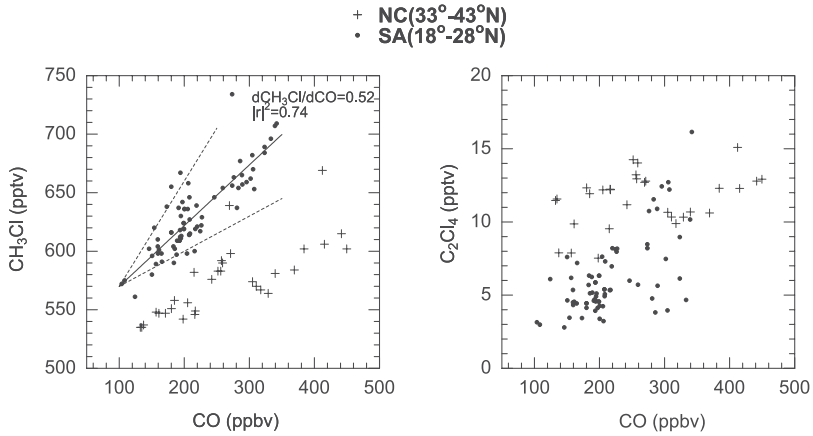

Figure 5. Scatter plots of CO-CH_3Cl (left) and CO-C_2Cl_4 (right) in the uplifted air masses, which originated at SA (solid circles) and NC (crosses) region. The dashed lines represent a typical range of the slopes in the biomass burning plumes [*Andreae et al.*, 1996].

convection, while others were transported by the WCB as the cyclone developed.

4.2.3. Dry Airstreams (DA)

[23] It is well established that downward transport of stratospheric air into the troposphere occurs behind cold fronts [e.g., *Danielsen*, 1968; *Shapiro et al.*, 1987]. A dry airstream is defined here as an airstream behind a surface cold front, originating in the upper troposphere or lower stratosphere at high latitude. Locations where DAs were observed at 5–9 km on this flight (Figure 7c) correspond to a dry region in the middle to upper troposphere over Japan (30°–45°N, 130°–145°E), as seen in Figure 6. Air masses in the DAs were characterized by high O_3 of 120–200 ppbv, low CO of 80–100 ppbv, and a low relative humidity of 2% (not shown). Figure 11a illustrates a cross section of potential vorticity (PV) calculated along the flight track with the observed O_3 values by the aircraft. A tongue of PV can clearly be seen extending downward to the mid-troposphere at 5 km and 139°–143°E, corresponding to the region of high O_3 values. The trajectories shown in Figure 11b confirm that the air masses in the DA were transported from high altitudes north of 55°N. Together, the PV map and TOMS total O_3 (not shown) clearly represent air masses of stratospheric origin associated with a dry intrusion.

[24] It is interesting to note that the DAs at 5–9 km were observed in the region adjacent to the air masses impacted by the COF at 10 km, as described in section 4.2.2. If these different types of air masses are mixed by turbulent mixing, the mixing ratios of trace gases such as O_3, NO_y, and H_2O in the resulting air masses can vary significantly depending on the degree of mixing. In fact, evidence of the mixing of stratospheric air with polluted air transported from the boundary layer has also been reported previously. *Prados et al.* [1999] showed that air masses behind a cold front, transported to the midtroposphere over Bermuda, were a mixture of stratospheric air and polluted air convected ahead of another cold front. *Parrish et al.* [2000] reported that highly polluted air was located in the immediate vicinity of air of stratospheric origin in the lower troposphere within a cyclone system over the western NAO. A key point of the current analysis is that the mixing of biomass burning effluents transported by convection with stratospherically influenced air could occur in the upper troposphere in the vicinity of the frontal region.

5. Partitioning and Export of NO_y Species

[25] In order to investigate the chemical evolution of NO_y species in the air masses vertically transported over the western Pacific, partitioning of NO_y is presented in this section for the WCB and COF identified in section 3. Figure 12 shows the median values of NO_x, PAN, and HNO_3 mixing ratios and their ratios to the total NO_y in the WCB and COF, as identified in section 3.2. The median values of the whole set of data obtained at the study area (22°–42°N and 122°–170°E) during TRACE-P are also shown in the figure for comparison. The NO_x mixing ratios and NO_x/NO_y ratios in the WCB and COF were much lower (10–30 pptv and 0.03) than the midlatitude median values (50–70 pptv and 0.10–0.15), particularly at 6–10 km. The NO_x/NO_y ratios in the WCB and COF were also lower than the median values of 0.10–0.30 in the continental air masses at 6–10 km over the western Pacific in February–March [*Kondo et al.*, 1997a]. Similarly, the HNO_3 mixing ratios (80 ± 10 pptv) and HNO_3/NO_y ratios (0.15 ± 0.05) in the WCB and COF were lower than the midlatitude median values (110 ± 10 pptv and 0.30 ± 0.05, respectively). In contrast, the PAN mixing ratios (330 ± 70 pptv) and the PAN/NO_y ratios (0.75 ± 0.10) in the WCB and COF were higher than the midlatitude median values (150 ± 50 pptv and 0.45 ± 0.05, respectively).

[26] NO_x is oxidized to HNO_3 by reaction with OH during daytime on a timescale of 1 day and by nighttime formation of N_2O_5 followed by hydrolysis on sulfate aerosols on a similar timescale [*Dentener and Crutzen*, 1993]. The residence time of air masses in the WCB and COF is 1–3 days, while chemical recycling from HNO_3 to NO_x occurs on a longer timescale of 10 days to several weeks [*Kley et al.*, 1981]. Therefore NO_x is not in chemical equilibrium with HNO_3 in these WCB and COF air masses. Moreover, the low HNO_3/NO_y ratios in

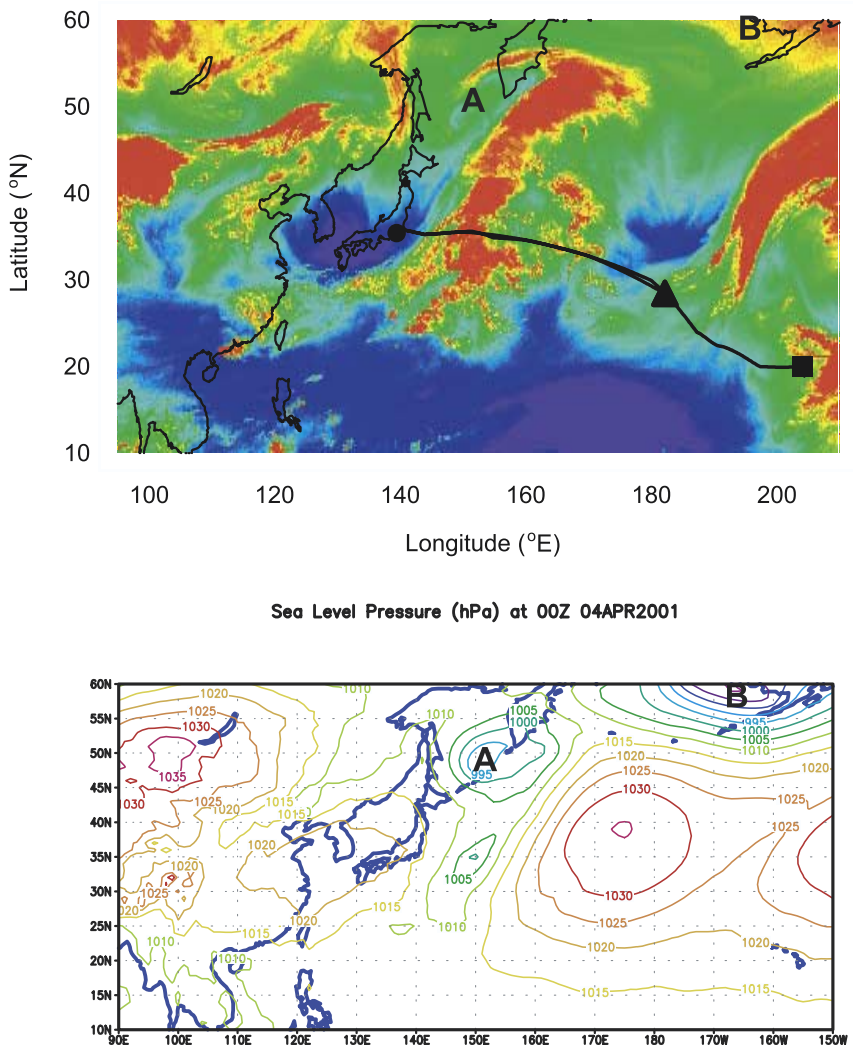

Figure 6. (top) GMS water vapor images (Infrared-3 channel) at 0400 UT on 4 April 2001 with flight tracks for the P-3B and DC-8 aircraft shown as black solid lines. Red represents a cloud region, while blue represents a cloud-free region or a relatively dry region. Locations of the centers of Cyclone-A and Cyclone-B are indicated as "A" and "B," respectively. Locations of Yokota AFB (solid circle), Midway (solid triangle), and Kona (solid square) are also plotted. (Bottom) Sea level pressure at 0000 UT on 4 April 2001.

the WCB and COF suggest that HNO_3 has been substantially removed during the vertical transport within 1–3 days, leading to the reduction of chemical recycling from HNO_3 to NO_x. In contrast, the midlatitude median values of NO_x increased with altitude at 6–12 km. This general increase of NO_x with altitude has typically been observed over the western Pacific [*Kondo et al.*, 1997a] and over other regions [*Kley et al.*, 1981; *Ridley et al.*, 1994], due to the longer chemical lifetime of NO_x and the input of in situ sources of NO_x in the upper troposphere such as lightning or aircraft emissions. The present results show that the air masses in the WCB and COF were isolated from ambient air and were less affected by such in situ sources of NO_x. To summarize, the lower NO_x/NO_y ratios in the WCB and COF are due to both the chemical imbalance between NO_x and HNO_3 and a small influence of in situ sources without significant mixing with surrounding air masses.

[27] The elevated PAN mixing ratios in the WCB and COF can be attributed to limited decomposition of the PAN produced over the biomass burning and industrial emissions region followed by the rapid upward transport of the air masses and limited mixing with surrounding air masses. Moreover, the dominance of PAN in NO_y was also due to the rapid loss of HNO_3 during transport by the WCB and COF, leading to the increase in the PAN/NO_y ratios. Loss of PAN during transport in the free troposphere should be very small due to the stability of PAN at low temperatures. In addition, wet deposition of PAN is negligible compared to HNO_3 because its solubility in water is small [*Kames et al.*, 1991]. PAN chemistry has only a minimal impact on net NO_x production of ±10% in the cold upper troposphere, as estimated using a 3-D CTM by *Moxim et al.* [1996]. However, the dominance of PAN in the WCB and COF can provide significant sources of NO_x in remote regions through long-range transport followed by descent to the

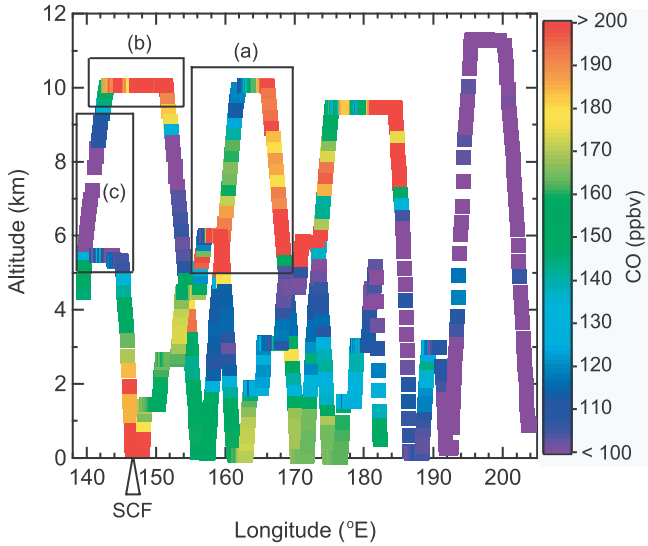

Figure 7. Vertical distributions of measured CO along the flight tracks of both the P-3B and DC-8 aircraft on 4 April 2001. The open triangle on the axis represents the location of a surface cold front (SCF) associated with Cyclone-A. Solid lines in the figure show locations where each airstream was identified.

warmer lower troposphere, where PAN decomposes to NO_x [*Moxim et al.*, 1996].

6. Removal of HNO_3 in the WCB and COF

[28] In this section, we estimate the export efficiency (EE) with which NO_y emitted from the surface over East Asia was transported to the sampling points by the WCB and COF. CO can serve as a good reference for estimating the NO_y removal rate [*Stohl et al.*, 2002], because CO is emitted simultaneously with NO_x and has a lifetime of 1–2 months. For the calculation of EE, the enhancement of NO_y and CO over their background level should be used [*Stohl et al.*, 2002]. In this analysis, the background mixing ratios of NO_y ($NO_{y(bkg)}$) and CO (CO_{bkg}) were determined to be 100 pptv and 80 ppbv, respectively, which are approximately the lowest values at 2–10 km over the study area (22°–42°N, 120°–170°E) during TRACE-P. The dNO_y and dCO can be then defined as $dNO_y = NO_y - NO_{y(bkg)}$ and $dCO = CO - CO_{bkg}$, respectively. The EE of NO_y can be derived from the slope of dNO_y/dCO ratios in each air mass by dividing it by the NO_x/CO emission ratios over the source regions. Molar ratios of NO_x/CO emitted over the SA and NC are estimated to be 0.034 ± 0.017 mol/mol and 0.051 ± 0.013 mol/mol, respectively, for the year 2000 (Figure 4) [*Streets et al.*, 2003]. Based on uncertainties in the CO (±156%) and NO_x (±23%) emissions estimations in China [*Streets et al.*, 2003], the overall uncertainty of the NO_x/CO ratios was estimated to be ±158%.

[29] Figure 13a shows a scatter plot of CO and NO_y in the WCB and COF air masses with reference data obtained at 2–11 km over the study area. The slopes of the regression lines for the WCB (3.15 pptv/ppbv) and COF (SA) (5.27 pptv/ppbv) show lower values compared to the reference data points between CO and NO_y over the study region. These lower slopes reflect large amounts of NO_y removal, as discussed below. On the other hand, the slope of the regression line for the COF (NC) showed a larger value of 10 pptv/ppbv. The difference of the slopes between the SA and NC categories can be attributed to (1) the removal rate during transport and/or (2) the difference of emission ratios over the two regions. Figure 13b also represents these scatter plots of CO against NO_y for the SA and NC with the expected fraction of the emission ratios. The EE value was estimated to be 9% in the WCB, while it was 15% (SA) and 19% (NC) in the COF. The results indicate that the WCB and COF transported 10–20% of NO_y emitted over the Asian continent to the free troposphere over the western Pacific. If the estimated uncertainties in the emissions ratios are given, the EE values range within 6–19% (WCB), 10–31% (COF-SA), and 13–26% (COF-NC). *Stohl et al.* [2002] showed only 3–5% of the NO_y emissions over the United States were transported above an altitude of 3 km over the North Atlantic, utilizing the aircraft data combined with a lagrangian transport model.

[30] It should be noted that EE includes the loss of NO_y in the boundary layer (z = 0–2 km) in addition to the removal during uplifted transport of air masses into the free troposphere (z = 2–12 km). In order to examine this process, the EE in the boundary layer near the source regions was

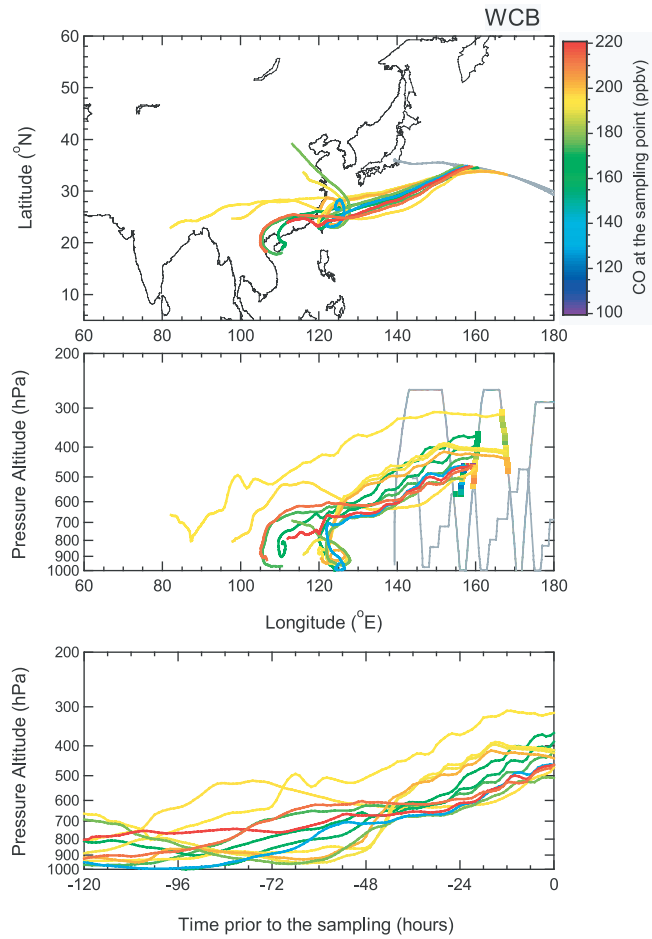

Figure 8. Five-day back trajectories, colored according to CO mixing ratios at the sampling points, representing the WCB on 4 April 2001. Gray lines in the middle panel show flight tracks for the P-3B and DC-8.

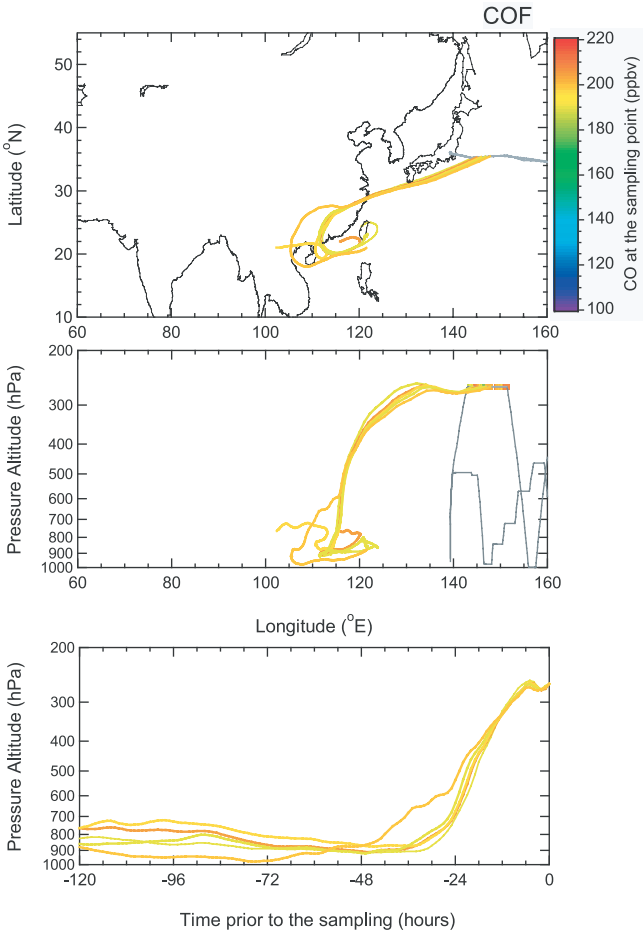

Figure 9. Same as Figure 8 but for the convective outflow associated with the stationary front over southeast China.

estimated. Air masses transported in the boundary layer within one day were selected based on trajectories calculated from the P-3B flight tracks on 7 and 9 March for the SA region and on 17 and 18 March for the NC region. The resulting number of trajectories was 17 for SA and 10 for NC. Figure 13b also includes scatter plots of CO and NO_y in these air masses of the selected boundary layer (BL) outflow. For the calculation of EE in the BL, CO_{bkg} and $NO_{y(bkg)}$ were determined to be 100 ppbv and 100 pptv, respectively, which are approximately the lowest values at 0–2 km over the study area. The EE values in these BL outflows for the SA and NC categories were estimated to be 33% and 30%, respectively. These BL outflows were likely affected by a much smaller subset of the source regions than the WCB and COF air masses. Given that source regions exhibit different emissions ratios, ranging from 0.038 (Southeast Asia) to 0.060 (China) [*Streets et al.*, 2003], the EE values in these BL outflows range over 19–33%. It should be noted, however, that these BL data were obtained only in limited cases and may not be representative. This is because concentrations of NO_y in the BL air masses are highly variable depending on variable occurrences of removal processes since emissions and because the emission estimates include initial uncertainties as described above. *Koike et al.* [2003] have made a similar estimate for NO_y of 15% (20–40%) at 2–7 km (0–2 km) transported from the

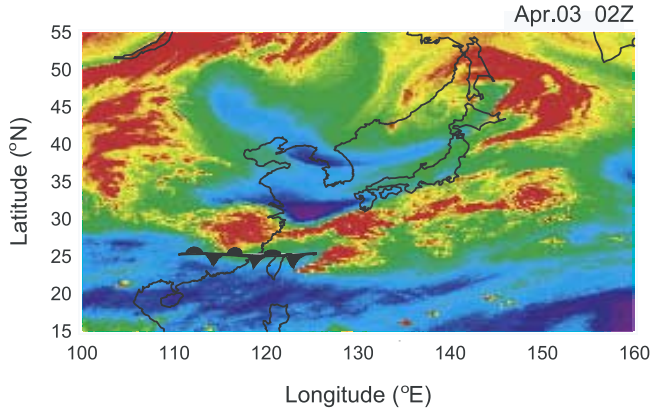

Figure 10. GMS water vapor image at 0200 UT on 3 April 2001, which corresponds to approximately one day prior to the observation. A stationary front is also shown, located over south China around 25°N.

northeast part of China to the Yellow Sea and Japan Sea during TRACE-P. These values are similar to those obtained in this study including the SA as a source region of NO_y.

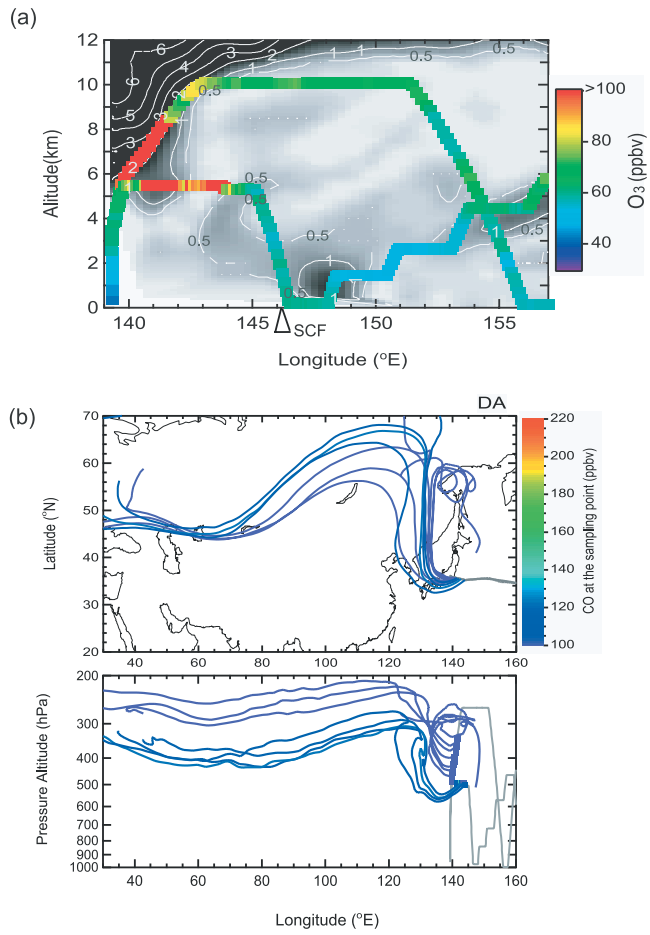

Figure 11. (a) Longitude-altitude cross section of the observed O_3 (colored) and PV (gray scale) along the flight tracks, where 1 PVU = 1×10^{-6} K·kg^{-1}·m^2·s^{-1}. The open triangle on the longitude axis represents the location of a surface cold front. (b) Same as Figure 8 but for the DA.

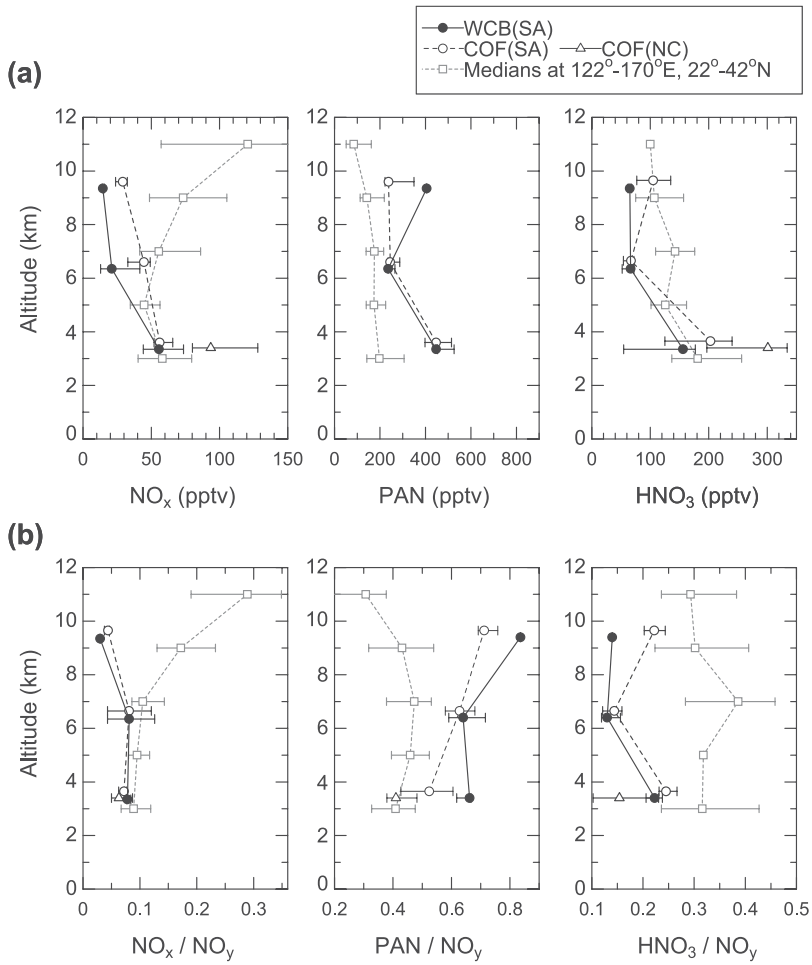

Figure 12. (a) Median values of NO_x, PAN, and HNO_3 in the WCB (solid circles) and COF for the SA (open circles) and NC (open triangles). Open squares show the median values of each species observed at 22°–42°N, 122°–170°E during the TRACE-P period. (b) Same as Figure 12a but for NO_x/NO_y, PAN/NO_y, and HNO_3/NO_y.

[31] Considering the EE value ranges of 10–20% for the WCB and COF at 2–10 km and 30% at 0–2 km, the results of this study suggest that there was additional NO_y removal during transport by the WCB and COF, by a factor of 1.5–3. This removal of NO_y, mainly due to HNO_3, occurred most likely by precipitation associated with warm frontal clouds or convective clouds (see Figure 1) during transport. In order to examine this, temporal and vertical variations of relative humidity are shown in Figure 14, which were derived from the ECMWF data along the trajectories for the WCB and COF on 4 April described in section 4. Altitude ranges where the relative humidity reached 100% were about 3–4 km and 2–4 km for the WCB and COF, respectively. These altitude ranges correspond to regions where precipitation had occurred. *Mari et al.* [2000] simulated that 70% of HNO_3 is efficiently scavenged by liquid precipitation in the lower (warm) part of the deep convective cloud below 7 km, by using a one-dimensional entraining/detraining plume model. The results of this study suggest that in addition to loss of HNO_3 in the BL, warm frontal clouds of the WCB as well as convective clouds provide an efficient sink for HNO_3, especially at lower altitudes in the free troposphere.

[32] For the EE estimation in this analysis, there is an assumption that the dNO$_y$/dCO ratios do not change due to dilution with constant dNO$_y$/dCO in an assumed background air. Even if the assumed CO_{bkg} value is 120 ppbv, which is the median value in the study area, the resulting EE values for each category increase by only 3%. This shows that the uncertainty of CO_{bkg} values does not significantly affect the estimates of EE values. Uncertainties of the EE estimates also include the possibility of additional inputs of NO_y during transport, such as lightning or aircraft emissions. However, as described in the previous section, the extremely low NO_x/NO_y ratios of less than 0.10 suggest that these additional inputs of NO_y were absent in both WCB and COF air masses. Therefore the influence of these additional sources of NO_y in the WCB and COF is considered negligible in the current analysis.

7. Summary and Conclusions

[33] We investigated the origins and pathways of synoptic-scale uplifted transport of pollutants and their effects on chemical distributions of NO_y species over the western Pacific, based on systematic aircraft measurements obtained

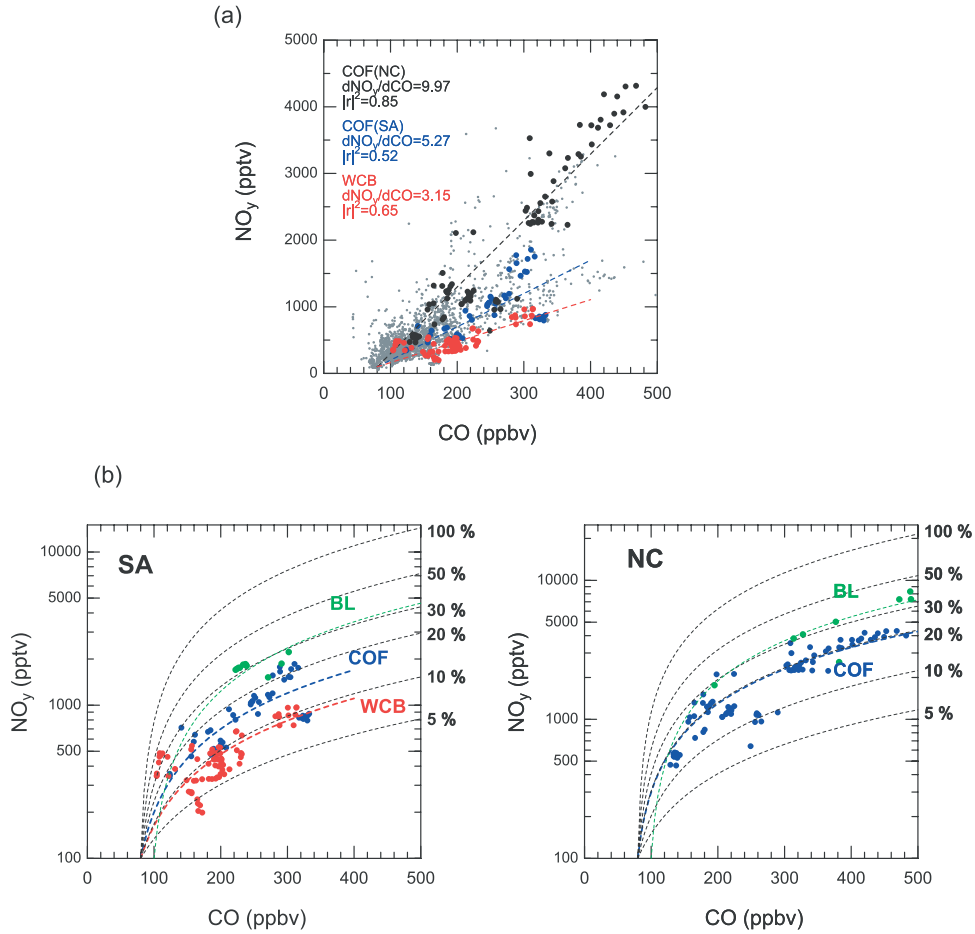

Figure 13. (a) Scatter plot of CO against NO_y for WCB (red), COF-SA (blue), and COF-NC (black) with linear fits for each category. The other values (gray) are data obtained at 2–11 km over the study area shown for reference. (b) Scatter plots of CO against NO_y for the SA (left) and NC (right) categories with the linear fits, as in Figure 13a. In addition, scatter plots between CO and NO_y in the BL outflow are plotted (green) for both SA and NC regions. Also shown are the expected relations for the emissions assuming a molar ratio of NO_y/CO of 0.034 and 0.051 for the SA and NC, respectively. The background CO (NO_y) mixing ratios at 2–11 km are determined to be 80 ppbv (100 pptv), while those at 0–2 km are determined to be 100 ppbv (100 pptv) over the study area.

during TRACE-P, in conjunction with 5-day back trajectories. During the observational season, convection and cyclones over East Asia to the western Pacific were attributed to more frequent incursions of warmer air from the south due to the building up of Pacific high pressure, compared to decreasing southward movement of cold air because of the weakening of the Siberian High by March.

[34] Vertically uplifted patterns of lagrangian transport from the Asian continent were selected by the trajectories calculated from sampling points along the 9 DC-8 and 6 P-3B flight tracks. Of these, 73% originated over Southeast Asia, where biomass burning was most active during this season, while 27% originated over northeast China. The SA-originating trajectories were associated with warm conveyor belts within midlatitude cyclones and convective outflow (COF) over southern China. The strong influence of biomass burning was confirmed by the higher mixing ratios of CO and CH_3Cl than the midlatitude median values, with a positive correlation of these species. On the other hand, the NC-originating trajectories were associated with convection within low-pressure systems. Air masses in the NC categories showed a large influence of fossil fuel combustion, revealed by higher mixing ratios of C_2Cl_4 compared to those in the SA categories.

[35] WCB and COF associated with a stationary front were identified for the 4 April case. The WCB and COF were found to originate in southern China, suggesting that air masses in the biomass burning region were transported by both the stationary front and WCB as the cyclone developed. The dry airstream, identified as originating from the tropopause region from the trajectory and PV analysis, was found to be located adjacent to the COF. Therefore turbulent mixing can produce air masses with combined chemical signatures of stratospherically influenced air masses and pollutants from biomass burning.

[36] The fractions of NO_x, PAN, and HNO_3 of the total NO_y in the WCB and COF were found to be different from the midlatitude median values. The NO_x levels were rela-

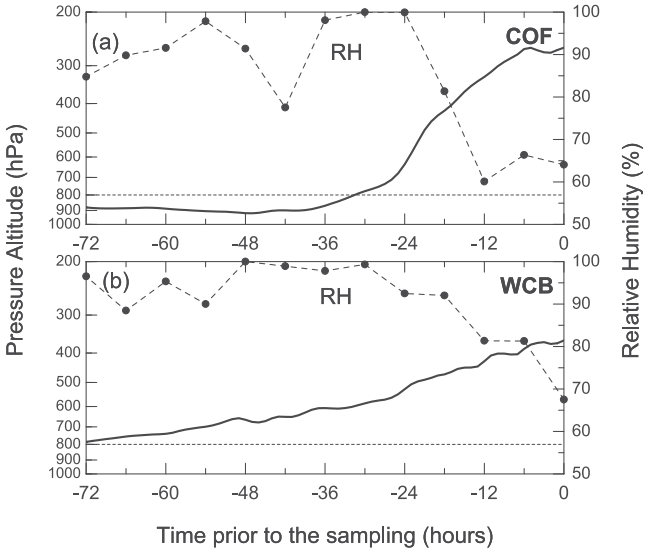

Figure 14. Temporal and vertical variations of relative humidity (RH) in the air mass along the back trajectories for the (a) COF and (b) WCB on 4 April. The RH was obtained from the ECMWF data within the 6-hour interval prior to sampling.

tively low both in the WCB and COF due to the chemical imbalance between NO_x and HNO_3 after the oxidation of a significant portion of the NO_x, as well as due to the small influence of in situ sources in the isolated air masses. PAN was found to be the dominant form of the NO_y in air masses transported by the WCB and COF. The high PAN/NO_y ratio can be due to the substantial production of PAN in the boundary layer of the biomass burning and industrial region and the lower temperature in the middle to upper troposphere. The WCB and COF can transport NO_x over long distances in the form of PAN to regions remote from Asian sources.

[37] The HNO_3/NO_y ratios in the WCB and COF were much lower than the midlatitude median values, indicating that HNO_3 was removed during transport within 1–3 days. Fractions of NO_y emitted from the surface over East Asia reaching the sampling points in the WCB and COF were estimated to be 10–20%. Similarly, fractions of NO_y transported within the boundary layer were estimated to be 30% for the SA and NC, although the amount of data collected was quite limited for each air mass category. The results suggest that a large amount of NO_y was removed during transport from the BL to the free troposphere. This was most likely due to loss of HNO_3 by precipitation during transport in the lower free troposphere in WCB and COF air masses, as well as loss of HNO_3 in the BL. A widespread region of precipitation over the east coast of the Asian continent to the North Pacific also suggests that the WCB and COF can provide an efficient sink for HNO_3 over the western Pacific.

[38] **Acknowledgments.** The TRACE-P mission was supported by the NASA Global Tropospheric Chemistry Program. The authors thank the crew of the NASA P-3B and DC-8 aircraft for their support. R. E. Newell and Y. Hu are acknowledged for providing PV values and a map of sea level pressure produced from ECMWF gridded data. The authors are grateful to H. Nakamura for helpful discussions on meteorology. Thanks also go to N. Oshima and Y. Morino for their assistance with the data analysis. Y. M. was supported by research fellowships of the Japan Society for the Promotion of Science for Young Scientists.

References

Andreae, et al., Trace gas and aerosol emissions from savanna fires, in *Biomass Burning and Global Change*, edited by J. S. Levine, pp. 278–295, MIT Press, Cambridge, Mass., 1996.

Bethan, S., G. Vaughan, C. Gerbig, A. Voltz-Thomas, H. Richer, and D. D. Tiddeman, Chemical air mass differences near fronts, *J. Geophys. Res.*, *103*, 13,413–13,434, 1998.

Bey, I., D. J. Jacob, J. A. Logan, and R. M. Yantosca, Asian chemical outflow to the Pacific: Origins, pathways and budgets, *J. Geophys. Res.*, *106*, 23,097–23,114, 2001.

Blake, N. J., D. R. Blake, B. C. Sive, T.-Y. Chen, J. E. Collins Jr., G. W. Sachse, B. E. Anderson, and F. S. Rowland, Biomass burning emissions and vertical distribution of atmospheric methyl halides and other reduced carbon gases in the south Atlantic Region, *J. Geophys. Res.*, *101*, 24,151–24,164, 1996.

Blake, N. J., et al., Large-scale latitudinal and vertical distribution of NMHCs and selected halocarbons in the troposphere over the Pacific Ocean during the March–April 1999 Pacific Exploratory Mission (PEM-Tropics B), *J. Geophys. Res.*, *106*, 32,627–32,644, 2001.

Browning, K. A., Organisation of clouds and precipitation in extratropical cyclones, in *Extratropical Cyclones—The Erik Palmen Memorial Volume*, Am. Meteorol. Soc., Boston, Mass., 1990.

Browning, K. A., and N. M. Roberts, Structure of a frontal cyclone, *Q. J.R. Meteorol. Soc.*, *122*, 1845–1872, 1994.

Chen, S.-J., Y.-H. Kuo, P.-Z. Zhang, and Q.-F. Bai, Synoptic climatology of cyclogenesis over east Asia, *Mon. Weather Rev.*, *119*, 1407–1418, 1991.

Chen, S.-J., Y.-H. Kuo, P.-Z. Zhang, and Q.-F. Bai, Climatology of explosive cyclones off the east Asian coast, *Mon. Weather Rev.*, *120*, 3029–3035, 1992.

Cooper, O. R., et al., Trace gas composition of midlatitude cyclones over the western North Atlantic Ocean: A conceptual model, *J. Geophys. Res.*, *107*(D7), 4056, doi:10.1029/2001JD000901, 2002a.

Cooper, O. R., et al., race gas composition of midlatitude cyclones over the western North Atlantic Ocean: A seasonal comparison of O_3 and CO, *J. Geophys. Res.*, *107*(D7), 4057, doi:10.1029/2001JD000902, 2002b.

Danielsen, E. F., Stratospheric-tropospheric exchange based on radioactivity, ozone and potential vorticity, *J. Atmos. Sci.*, *25*, 502–518, 1968.

Dentener, F. J., and P. J. Crutzen, Reaction of N_2O_5 on tropospheric aerosols: Impact on the global distributions of NO_x, O_3, and OH, *J. Geophys. Res.*, *98*, 7149–7163, 1993.

Duncan, B. N., R. V. Martin, A. C. Staudt, R. Yevich, and J. A. Logan, Interannual and seasonal variability of biomass burning emissions constrained by satellite observations, *J. Geophys. Res.*, *108*(D2), 4100, doi:10.1029/2002JD002378, 2003.

Ferriday, J. G., and S. K. Avery, Passive remote sensing of rainfall with SSM/I: Algorithm development and implementation, *J. Appl. Meteorol.*, *33*, 1587–1596, 1994.

Fuelberg, H. E., et al., TRACE A Trajectory intercomparison: 2. Isentropic and kinematic methods, *J. Geophys. Res.*, *101*, 23,927–23,939, 1996.

Fuelberg, H. E., C. M. Kiley, J. R. Hannan, D. J. Westberg, M. A. Avery, and R. E. Newwell, Atmospheric transport during the Transport and Chemical Evolution over the Pacific (TRACE-P) experiment, *J. Geophys. Res.*, *108*(D20), 8782, doi:10.1029/2002JD003092, in press, 2003.

Grant, W. B., et al., A case study of transport of tropical marine boundary layer and lower tropospheric air masses to the northern midlatitude upper troposphere, *J. Geophys. Res.*, *105*, 3757–3769, 2000.

Jacob, D. J., et al., The transport and chemical evolution over the Pacific (TRACE-P) aircraft mission: Design, execution, and first results, *J. Geophys. Res.*, *108*(D20), 8781, doi:10.1029/2002JD003276, in press., 2003.

Kames, J., S. Shweighoefer, and U. Schurath, Henry's Law constant and hydrolysis of peroxyacetyl nitrate, *J. Atmos. Chem.*, *12*, 169–180, 1991.

Kley, D., J. W. Drummomd, M. McFarland, and S. C. Liu, Tropospheric profiles of NO_x, *J. Geophys. Res.*, *86*, 3153–3161, 1981.

Koike, M., et al., Impact of aircraft emissions on reactive nitrogen over the North Atlantic flight corridor region, *J. Geophys. Res.*, *105*, 3665–3677, 2000.

Koike, M., et al., Impact of anthropogenic reactive nitrogen and sulfur compounds from the East Asia region in spring, *J. Geophys. Res.*, *108*(D20), 8789, doi:10.1029/2002JD003284, in press., 2003.

Kondo, Y., M. Koike, S. Kawakami, H. B. Singh, H. Nakajima, G. L. Gregory, D. R. Blake, G. W. Sachse, J. T. Merrill, and R. E. Newell, Profiles and partitioning of reactive nitrogen over the Pacific Ocean in winter and early spring, *J. Geophys. Res.*, *102*, 28,405–28,424, 1997a.

Kondo, Y., S. Kawakami, M. Koike, D. W. Fahey, H. Nakajima, N. Toriyama, M. Kanada, Y. Zhao, G. W. Sachse, and G. L. Gregory, The performance of an aircraft instrument for the measurement of NO_y, *J. Geophys. Res.*, *102*, 28,663–28,671, 1997b.

Kowol-Santen, J., M. Beeekman, S. Schmitgen, and K. Dewey, Tracer analysis of transport from the boundary layer to the free troposphere, *Geophys. Res. Lett.*, *28*, 2907–2910, 2001.

Liang, J., L. W. Horowitz, D. J. Jacob, Y. Wang, A. M. Fiore, J. A. Logan, G. M. Gardner, and J. W. Munger, Seasonal budgets of reactive nitrogen species and ozone over the United States, and export fluxes to the global atmosphere, *J. Geophys. Res.*, *103*, 13,435–13,450, 1998.

Mari, C., D. J. Jacob, and P. Bechtold, Transport and scavenging of soluble gases in a deep convective cloud, *J. Geophys. Res.*, *105*, 22,255–22,267, 2000.

Mauldin, R. L., III, D. J. Tanner, and F. L. Eisele, A new chemical ionization mass spectrometer technique for the fast measurement of gas phase nitric acid in the atmosphere, *J. Geophys. Res.*, *103*, 3361–3367, 1998.

Miyazaki, Y., K. Kita, Y. Kondo, M. Koike, M. Ko, W. Hu, S. Kawakami, D. R. Blake, and T. Ogawa, Springtime photochemical ozone production observed in the upper troposphere over East Asia, *J. Geophys. Res.*, *108*(D3), 8398, doi:10.1029/2001JD000811, 2002.

Moxim, W. J., H. Levy II, and P. S. Kasibhatla, Simulated global tropospheric PAN: Its transport and impact on NO_x, *J. Geophys. Res.*, *101*, 12,621–12,638, 1996.

Nieuwolt, S., *Tropical Climatology: An Introduction to the Climates of the Low Latitudes*, John Wiley, New York, 1977.

Parrish, D. D., J. S. Holloway, R. Jakoubek, M. Trainer, T. B. Ryerson, G. Hubler, F. C. Fehsenfeld, J. L. Moody, and O. R. Cooper, Mixing of anthropogenic pollution with stratospheric ozone: A case study from the North Atlantic wintertime troposphere, *J. Geophys. Res.*, *105*, 24,363–24,374, 2000.

Prados, A. I., R. R. Dickerson, B. G. Doddridge, P. A. Milne, J. L. Moody, and J. T. Merrill, Transport of ozone and pollutants from North America to the North Atlantic Ocean during the 1996 AEROCE Intensive Experiment, *J. Geophys. Res.*, *104*, 26,219–26,234, 1999.

Ridley, B. A., J. G. Walega, J. E. Dye, and F. E. Grahek, Distributions of NO, NO_x, NO_y, and O_3 to 12 km altitude during the summer monsoon season over New Mexico, *J. Geophys. Res.*, *99*, 25,519–25,534, 1994.

Rudolph, J., A. Khedim, R. Koppmann, and B. Bonsang, Field study of the emissions of methyl chloride and other halocarbons from biomass burning in Western Africa, *J. Atmos. Chem.*, *22*, 67–80, 1995.

Sachse, G. W., G. F. Hill, L. O. Wade, and M. G. Perry, Fast response, high-precision carbon monoxide sensor using a tunable diode laser absorption technique, *J. Geophys. Res.*, *92*, 2071–2081, 1987.

Sandholm, S., J. D. Bradshaw, K. S. Dorris, M. O. Rogers, and D. D. Davis, An airborne-compatible photofragmentation two-photon laser-induced fluorescence instrument for measuring background tropospheric NO, NO_x, and NO_2, *J. Geophys. Res.*, *95*, 10,155–10,161, 1990.

Shapiro, M. A., T. Hampel, and A. J. Krueger, The Arctic tropopause fold, *Mon. Weather Rev.*, *115*, 444–454, 1987.

Simpson, I. J., N. J. Blake, E. Atlas, F. Flocke, J. H. Crawford, H. E. Fuelberg, C. M. Kiley, F. S. Rawland, and D. R. Blake, Photochemical production and evolution of selected C2-C5 alkyl nitrates in tropospheric air influenced by Asian outflow, *J. Geophys. Res.*, *108*(D20), 8808, doi:10.1029/2002JD002830, in press, 2003.

Singh, H. B., et al., Reactive nitrogen and ozone over the western Pacific: Distribution, partitioning, and sources, *J. Geophys. Res.*, *101*, 1793–1808, 1996.

Singh, H. B., et al., Latitudinal distribution of reactive nitrogen in the free troposphere over the Pacific Ocean in late winter/early spring, *J. Geophys. Res.*, *103*, 28,237–28,246, 1998.

Stohl, A., A 1-year Lagrangian "climatology" of airstreams in the Northern Hemisphere troposphere and lowermost stratosphere, *J. Geophys. Res.*, *106*, 7263–7279, 2001.

Stohl, A., and T. Trickl, A textbook example of long-range transport: Simultaneous observation of ozone maxima of stratospheric and North American origin in the free troposphere over Europe, *J. Geophys. Res.*, *104*, 30,445–30,462, 1999.

Stohl, A., G. Wotawa, P. Seibert, and H. Kromp-Kolb, Interpolation errors in wind fields as a function of spatial and temporal resolution and their impact on different types of kinematic trajectories, *J. Appl. Meteorol.*, *34*, 2149–2165, 1995.

Stohl, A., M. Trainer, T. B. Ryerson, J. S. Holloway, and D. D. Parrish, Holloway, and D .D. Parrish, Export of NO_y from the North American boundary layer during 1996 and 1997 North Atlantic Regional Experiments, *J. Geophys. Res.*, *107*(D11), 4131, doi:10.1029/2001JD000519, 2002.

Streets, D. G., et al., A year-2000 inventory of gasses of gaseous and primary aerosol emissions in Asia to support TRACE-P modeling and analysis, *J. Geophys. Res.*, *108*(D21), 8809, doi:10.1029/2002JD003093, in press., 2003.

Talbot, R. W., et al., Large-scale distributions of tropospheric nitric, formic, and acetic acids over the western Pacific basin during wintertime, *J. Geophys. Res.*, *102*, 28,303–28,313, 1997.

Talbot, R. W., et al., Reactive nitrogen in Asian continental outflow over the western Pacific: Results from the NASA TRACE-P airborne mission, *J. Geophys. Res.*, *108*(D20), 8803, doi:10.1029/2002JD003129, in press., 2003.

Wang, C. J. L., D. R. Blake, and F. S. Rowland, Seasonal variations in the atmospheric distribution of a reactive chlorine compound, tetrachloroethene ($CCl_2 = CCl_2$), *Geophys. Res. Lett.*, *22*, 1097–1100, 1995.

Wernli, H., and H. C. Davis, A Lagrangian-based analysis of extratropical cyclones, I, The method and some applications, *Q.J.R. Meteorol. Soc.*, *123*, 467–489, 1997.

M. A. Avery and G. W. Sachse, Chemistry and Dynamics, NASA Langley Research Center, Hampton, VA 23681, USA. (m.a.avery@larc.nasa.gov; g.w.sachse@larc.nasa.gov)

D. R. Blake, Department of Chemistry, University of California, Irvine, CA 92697, USA. (drblake@uci.edu)

F. L. Eisele, F. Flocke, A. J. Weinheimer, and M. Zondlo, Atmospheric Chemistry Division, National Center for Atmospheric Research, Boulder, CO 80303. USA. (eisele@ncar.ucar.edu; ffl@acd.ucar.edu; wein@ucar.edu; zondlo@ucar.edu)

H. E. Fuelberg and C. M. Kiley, Department of Meteorology, Florida State University, Tallahassee, FL 32306, USA. (fuelberg@huey.met.fsu.edu; ckiley@met.fsu.edu)

K. Kita, Department of Environmental Science, Ibaraki University, Bunkyo 2-1-1, Mito, Ibaraki, 310-8512, Japan. (kita@env.sci.ibaraki.ac.jp)

M. Koike, Earth and Planetary Science, Graduate School of Science, University of Tokyo, Tokyo, 113-0033, Japan. (koike@eps.s.u-tokyo.ac.jp)

Y. Kondo, Y. Miyazaki, and N. Takegawa, Research Center for Advanced Science and Technology, University of Tokyo, 4-6-1 Komaba, Meguro-ku, Tokyo, 153-8904, Japan. (kondo@atmos.rcast.u-tokyo.ac.jp; yuzom@atmos.rcast.u-tokyo.ac.jp; takegawa@atmos.rcast.u-tokyo.ac.jp)

S. T. Sandholm, Georgia Institute of Technology, Atlanta, Georgia 30332, USA. (scott.sandholm@eas.gatech.edu)

H. B. Singh, NASA Ames Research Center, Moffet Field, CA 94035, USA. (hsingh@mail.arc.nasa.gov)

R. W. Talbot, University of New Hampshire, Durham, NH 03820, USA. (robert.talbot@unh.edu)